

# Large-Scale Testing of Shallow Ground Improvements using Controlled Staged-Loading with T-Rex

S. van Ballegooy<sup>1</sup>, J.N. Roberts<sup>2</sup>, K.H. Stokoe<sup>3</sup>, B.R. Cox<sup>4</sup>, F.J. Wentz<sup>5</sup>, S. Hwang<sup>6</sup>

## ABSTRACT

Ishihara (1985) recognised that a thick non-liquefying crust overlying liquefying soils would reduce the consequences of liquefaction (i.e., sand boils, loss of bearing capacity and differential settlement). In Christchurch, in the aftermath of the 2010-2011 Canterbury earthquakes, detailed engineering assessments of nearly 60,000 single-family houses combined with a comprehensive regional scale geotechnical investigation, clearly showed that less structural damage occurred in liquefaction-prone areas containing an intact, relatively stiff non-liquefying crust with a minimum thickness of approximately 3 m. To increase the resilience of the post-earthquake rebuilt/repairs Christchurch residential housing stock, the use of shallow (i.e.,  $\leq 4$  m deep) ground improvements to construct a stiff, non-liquefying crust and mitigate the consequences of underlying liquefaction was evaluated. In this paper, the results from the in-situ vibroseis dynamic (T-Rex) load testing are presented. This testing was able to examine the potential for liquefaction triggering to a depth of about 3 to 4 m below the ground surface, coinciding with the target depth of the ground improvement methods investigated as part of this study. The shake testing of the ground improvement panels demonstrated that, in general, where the shallow ground improvements increased the Cone Penetration Test (CPT) tip resistance ( $q_c$ ) or the composite crosshole shear wave velocity ( $V_s$ ) of the improved ground relative to the natural soil, there was a corresponding reduction in the maximum cyclic shear strain ( $\gamma$ ) induced in the improved soil increasing the liquefaction resistance.

## Introduction

The 2010 – 2011 Canterbury Earthquake Sequence (CES) caused widespread liquefaction-related land and building damage (described in Rogers et al., 2015), affecting 51,000 residential properties in Christchurch, including 15,000 residential houses damaged, beyond economical repair. In the suburbs most vulnerable to liquefaction damage, the CES revealed the importance of constructing robust, stiffened foundations capable of resisting the damaging effects of future liquefaction (i.e. angular distortion, lateral stretch and loss of ground support) or the need to undertake ground improvements to mitigate the damage caused by future liquefaction in future earthquakes. Therefore, the New Zealand Earthquake Commission (EQC) funded an extensive shallow ground improvement trial program to evaluate the efficacy of various shallow ground improvement methods and determine the cost by undertaking full-scale construction trials on residential properties. The purpose was to investigate and determine whether there are practical cost effective shallow ground improvement methods that could be constructed on properties in

---

<sup>1</sup>Senior Geotechnical Engineer, Tonkin & Taylor Ltd, Auckland, New Zealand, [svanBallegooy@tonkin.co.nz](mailto:svanBallegooy@tonkin.co.nz)

<sup>2</sup>Graduate Research Asst., Civil, Arc. & Env. Eng., Uni. of Texas at Austin, Austin, USA, [jnroberts@utexas.edu](mailto:jnroberts@utexas.edu)

<sup>3</sup>Professor, Civil, Arc. & Env. Eng., Uni. of Texas at Austin, Austin, USA, [k.stokoe@mail.utexas.edu](mailto:k.stokoe@mail.utexas.edu)

<sup>4</sup>Professor, Civil, Arc. & Env. Eng., Uni. of Texas at Austin, Austin, USA, [brcox@utexas.edu](mailto:brcox@utexas.edu)

<sup>5</sup>Principal, Wentz-Pacific Ltd, Napier, New Zealand, [rwentz@wp-geo.co.nz](mailto:rwentz@wp-geo.co.nz)

<sup>6</sup>Graduate Research Asst., Civil, Arc. & Env. Eng., Uni. of Texas at Austin, Austin, USA, [syongmoon@utexas.edu](mailto:syongmoon@utexas.edu)

existing residential areas to form and/or enhance a non-liquefying crust and reduce liquefaction vulnerability. The methods tested included Rapid Impact Compaction (RIC), Rammed Aggregate Pier™ (RAP) reinforcement, Driven Timber Poles (DTP), Low Mobility Grout (LMG), Resin Injection (RES), Gravel Rafts (GR), Soil-Cement Rafts (SCR) and Horizontal Soil-Cement Mixed (HSM) beams. The construction methodology of each of the tested ground improvement methods is described in van Ballegooy et al. (2015).

Construction of the various shallow ground improvement methods was undertaken in three different locations in Christchurch (Sites 3, 4 and 6) in the areas most severely affected by liquefaction. (The location of the sites is shown in Wissmann et al., 2015.) The testing phase of the shallow ground improvement trials comprised pre- and post-improvement Cone Penetration Testing (CPT), seismic crosshole testing, vibroseis T-Rex testing and blast-induced liquefaction testing. In order to assess the overall effectiveness of the shallow ground improvements to mitigate the damaging effects of liquefaction, an investigation of two primary mechanisms need to be investigated: (1) how effective the improvements are in preventing or limiting the triggering of liquefaction; and (2) how effective they are in reducing the consequences if liquefaction triggering occurs in the soil beneath the improved zone.

The peak cyclic shear strain ( $\gamma$ ) profiles produced by vibroseis T-Rex testing indicated that, at a depth of approximately 4 m, the maximum  $\gamma$  at all test panels was consistently  $< 0.02\%$ . Research by Dobry et al. (1982) has shown that excess pore water pressures ( $r_u$ ) do not develop until the peak  $\gamma$  are greater than  $0.01\%$  (the threshold  $\gamma$ ), and this finding is consistent with the results from this study. Therefore, it was demonstrated that vibroseis T-Rex testing was only able to examine the liquefaction triggering to a depth of about 3 to 4 m below the ground surface, which is the target depth of improvement in this study. Essentially, vibroseis T-Rex testing was used to examine the effectiveness of the various ground improvement methods to develop a non-liquefying crust (i.e., the  $H_1$  layer described in Ishihara, 1985). However, because vibroseis T-Rex is unable to induce liquefaction beneath the improvement zone, blast-induced liquefaction trials were also undertaken (described in Wentz et al., 2015) to examine performance of different shallow ground improvements in mitigating differential settlement caused by liquefaction of the underlying unimproved soil layers (i.e., the  $H_2$  layer described in Ishihara, 1985).

Vibroseis T-Rex testing was applied to ground improvement test panels composed of Natural Soil (NS), RIC, RAP, DTP, LMG, RES and HSM beams. Shake testing of the GR and SCR ground improvement test panels were not undertaken because these materials will not liquefy and hence there was no need to assess their triggering potential. Due to space constraints in this paper, only the results of the RIC, RAP and LMG ground improvements compared to the natural soil are discussed. Wissman et al. (2015) and Wansbone et al. (2015) examine the vibroseis T-Rex testing of the RAP and HSM beam ground improvements in greater depth. Schematics of the construction of the RIC, RAP and LMG methods is shown in Figure 1.

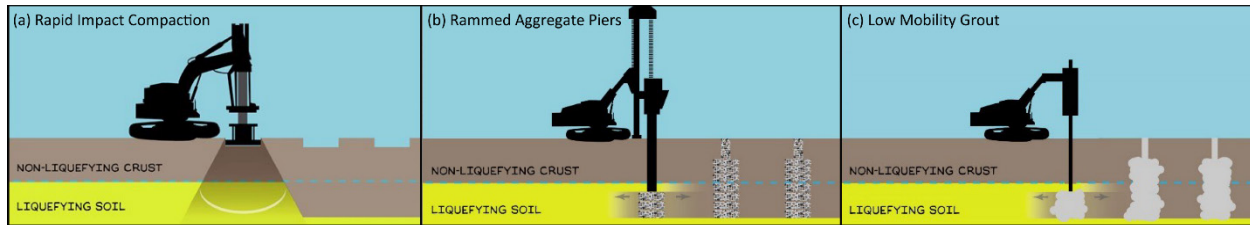


Figure 1. Illustration of the RIC, RAP and LMG ground improvement methods.

### Vibroseis T-Rex Testing Methodology

The T-Rex truck applies a vertical load of 245 kN to a 2.3-m square baseplate that is set on the ground, resulting in a pressure of 46 kPa on the ground surface beneath the baseplate. At each test panel, the T-Rex truck applied a horizontal cyclic load at the ground surface using a 10-Hz frequency for 100 cycles (10 seconds of shaking,  $N = 100$ ). The testing typically involved five loading stages, starting from the lowest level of loading ( $\pm 13$  kN) to the highest level ( $\pm 107$  or  $\pm 133$  kN). A horizontal cyclic load of  $\pm 133$  kN is equal to  $\pm 25$  kPa cyclic shear stress imparted on the soil at the ground surface. In the maximum loading stage at the natural (unimproved) soil test panels, this cyclic loading induces a  $\gamma$  of approximately 0.3% in the ground beneath the baseplate at a depth of about 1 m, reducing to around 0.05% at a depth of approximately 3 m.

The soil response was recorded with embedded two dimensional (2D) velocity transducers and Pore Pressure Transducers (PPTs). The induced  $\gamma$  at specific locations were evaluated from relative displacements between adjacent sensor locations. The pore pressure generation was directly measured with PPTs. Thus, the coupled behaviour between the dynamic response of the soil skeleton, represented by  $\gamma$ , and the generated pressure was recorded. These measurements were collected over a range of applied shaking levels in both natural and improved soils.

A typical test and instrumentation layout for the test panels is shown in Figure 2 (RAP in this case). Note that the twelve RAP columns shown in Figure 2b are located in the centre of the 7 by 7 m test panel which contained 22 columns. The location of the T-Rex baseplate during testing and the direction of shaking are shown in plan view in Figure 2b and cross-sectional perspectives are shown in Figures 2c and 2d. Before performing the shaking tests, instrumentation was embedded within the plan footprint (2.3 x 2.3 m) of the baseplate at each test panel. The instrumentation was installed using a CPT pushing mechanism mounted on the back of the T-Rex truck. The typical instrumentation array in the test panels, which consisted of four, 2D velocity transducers and five PPTs, is shown in a plan in Figure 2b and in cross section in Figure 2d.

### Reduction of Test Results and Discussion

The raw data collected from the sensor arrays during vibroseis T-Rex testing consists of velocity and pore pressure time histories at each sensor location. These data were used to compute the  $r_u$  (the ratio of generated pore water pressure to the initial vertical effective stress including the static vertical load imparted by the T-Rex baseplate;  $r_u = \Delta u / \sigma_v'$ ) time history and the induced  $\gamma$

time history. An example of these time histories is shown in Figure 2e, corresponding to measurements at a depth of 2.1 m at one of the natural soil panels at Site 6 for an applied horizontal cyclic loading of 107 kN (~20 kPa applied horizontal cyclic stress at the ground surface). The velocity time histories were numerically integrated to obtain displacement time histories, which were then used to evaluate  $\gamma$  development. The  $\gamma$  histories at each PPT location were calculated using the displacement-based method as described by Cox et al. (2009).

The maximum  $\gamma$  for each loading stage was linearly adjusted slightly to a nominal level of applied shear stress at the ground surface so that the  $\gamma$  for each of the tested ground improvement panels could be directly compared. For example, the peak shear stress imparted by the T-Rex vibroseis unit at the ground surface during the second loading stage of the natural soil test panel at Site 6 was recorded as 5.3 kPa; therefore, the estimated peak  $\gamma$  for this loading stage were multiplied by a ratio of 5 kPa : 5.3 kPa to linearly adjust the  $\gamma$  to match a nominal shear stress value for comparison across test panels. A nominal shear stress level is used because while the input signal sent to T-Rex vibroseis unit is set at a consistent value for each test panel (e.g. 1.5, 5, 10, 15, 20 and 25 kPa), the true force output depends on the stiffness of the soil as well as various nonlinearities in the electrical and mechanical systems relating to the operation of the T-Rex vibroseis unit.

The last two columns of Figure 3 plot the adjusted  $\gamma$  values (at the 5 and 15 kPa applied cyclic stresses at the ground surface) at each PPT location with depth. The blue, yellow, green and red lines represent the two nominal shear stress profiles for the natural soil panel and the RIC, RAP and LMG ground improvement panels, respectively.

Pre- and post-improvement CPT and crosshole testing was undertaken at each of the ground improvement panels as well as the natural soil panels. The location of the crosshole testing relative to the ground improvement aggregate columns or grout bulbs is shown in Figure 2a. For the RAP and LMG ground improvements, two set of compression wave velocity ( $V_P$ ) and shear wave velocity ( $V_S$ ) measurements were made: (1) between the improvement zones and (2) across the improvement zones. The crosshole testing methodology is described in Stokoe et al. (2014).

The CPT tip resistance ( $q_c$ ) and soil behavior type index ( $I_c$ ) traces are shown on the first two columns on the left of Figure 3, respectively. Likewise the crosshole  $V_P$  and  $V_S$  traces are shown on the third and fourth columns from the left, respectively, and the corresponding small-strain shear modulus ( $G_{max}$ ) profiles calculated from the  $V_S$  profiles are shown in the fifth column from the left. Similar to the nominal shear stress  $\gamma$  profiles, the blue, yellow, green and red lines represent the profiles for the natural soil, RIC, RAP and LMG test panels, respectively. For the RAP and LMG ground improvements, the dark green and dark red traces represent the measured  $V_P$  and  $V_S$  across the improvement zone and the light green and light red traces represent the measured  $V_P$  and  $V_S$  between the improvement zones, respectively.

The results in Figure 3 show that, in general, the RAP ground improvement is the most effective in increasing the CPT  $q_c$  (which directly correlates with an increase in the Cyclic Resistance Ratio, CRR) when  $I_c < 1.8$ . The RIC ground improvement is also effective in increasing the  $q_c$  when  $I_c < 1.8$ . Little to no increase in  $q_c$  was observed for the RIC and RAP ground improvements when  $I_c > 1.8$ , nor for the LMG ground improvement at any  $I_c$  value.

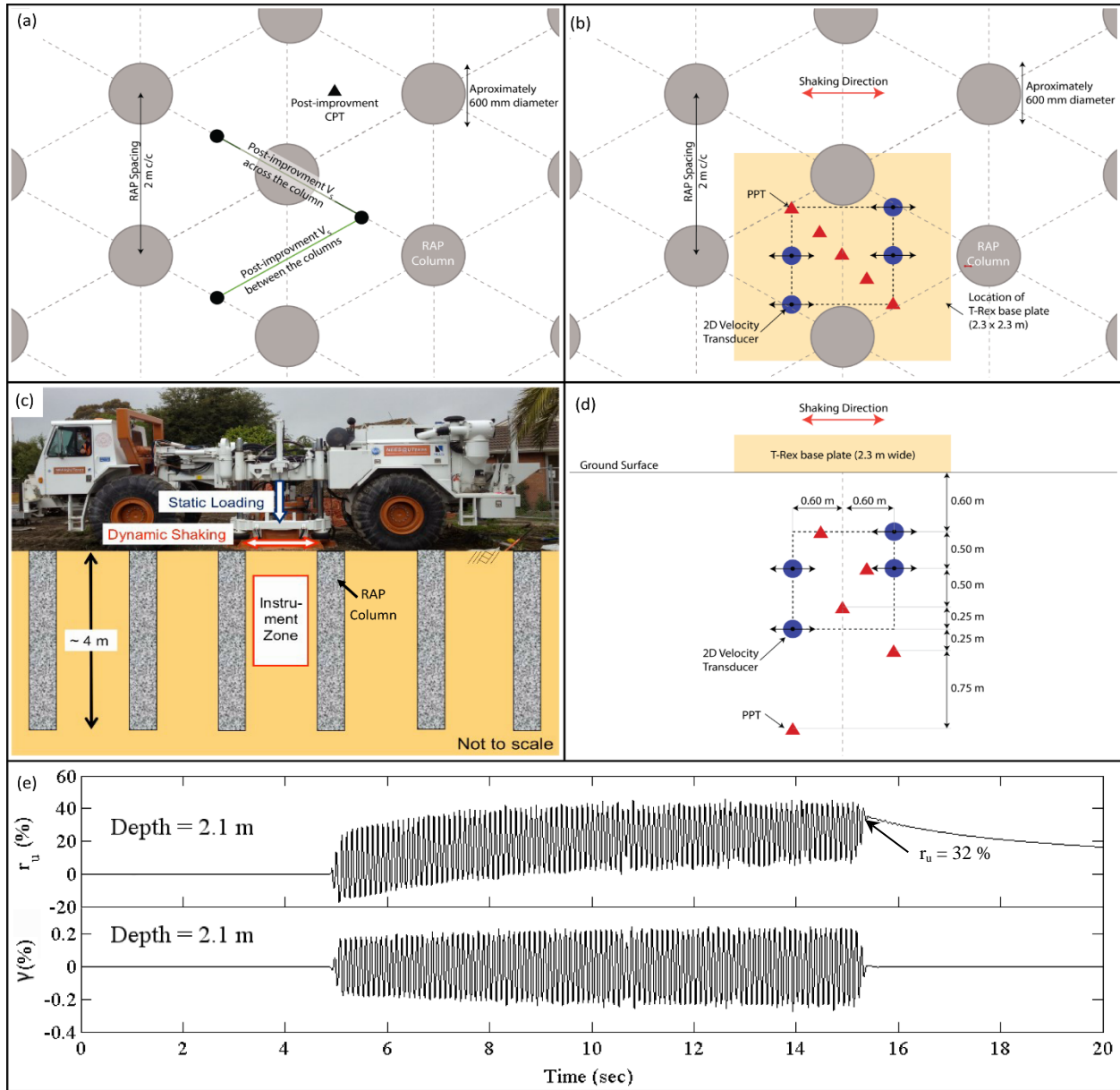


Figure 2. (a) Location of the CPT and crosshole  $V_p$  and  $V_s$  testing relative to the RAP columns. (b & d) The relative horizontal and vertical location, respectively, of the sensors beneath the T-Rex baseplate relative to the RAP columns. (c) Schematic cross section of the T-Rex truck on the RAP test panel during shaking. (e) Time histories of  $r_u$  and  $\gamma$  from data recorded at a depth of 2.1 m at one of the natural soil panels (not the RAP panel) at Site 6.

For both the RAP and the RIC ground improvements, the crosshole-measured  $V_s$  between the improvement zones show some improvement on a site-by-site basis relative to the natural ground. Furthermore, the crosshole  $V_s$  measured between the LMG bulbs appears to have decreased relative to the natural ground. Within the RAP ground improvement, however, the composite  $V_s$  (measured across the RAP columns) is significantly larger than those for both

unimproved and improved soil because of the presence of the stiff RAP elements. In comparison with the natural soil, the average composite  $G_{\max}$  values (calculated from the composite  $V_S$ ) increased by approximately 15 MPa (~40% increase) within the upper silty soil horizon and by approximately 65 MPa (~130% increase) within the lower clean sand soil horizon. Unlike the CPT results that indicated negligible improvement in the upper siltier soils (with  $I_c > 1.8$ ), the clear improvement in  $G_{\max}$  in these soil layers suggests the potential for reduced liquefaction potential. Similar trends are observed for the crosshole-measured  $V_S$  across the LMG bulbs, but it is noted that this increased stiffness across the bulbs is irregular, mainly because the LMG bulbs themselves are irregular and not continuous.

The  $\gamma$  profiles from vibroseis T-Rex testing decay relatively rapidly with depth because the T-Rex truck applies shear loads at the ground surface. For both load cases shown in Figure 3 (i.e. the 5 and 15 kPa of applied cyclic horizontal stress at the ground surface), the standardised  $\gamma$  profiles do not show any noticeable reduction in  $\gamma$  compared to the natural soil for both the RIC and LMG ground improvement methods. However, the results for the RAP ground improvement indicate that for each of the applied shear stress levels, the  $\gamma$  profiles in the RAP reinforced soil were reduced by approximately 60% to 80% relative to the natural soil, which indicates that the composite RAP reinforced ground is stiffer than the natural soil by a factor ranging from 3 to 5. The increase in composite stiffness (indicated by the crosshole  $V_S$  across the RAP columns) decreases the  $\gamma$  and hence the potential for development of  $r_u$  (as shown by Stokoe et al., 2014), increasing liquefaction triggering resistance under cyclic loading. The likely reason that the reduction in  $\gamma$  for the same applied loading was not seen in the LMG (even though the measured crosshole  $V_S$  across the LMG bulbs is higher) is because the LMG bulbs were not regular continuous reinforcing elements to stiffen the overall response of the ground, but instead they were a series of irregular discontinuous bulbs and planes based on visual observation during exhuming investigations at the end of the ground improvement trial program (van Ballegooy et al., 2015).

It is important to note that Stokoe et al. (2014) make direct comparisons between measured parameters for the ground improvement panels and the adjacent natural soil measured parameters at Site 6. Therefore, their conclusions relate specifically to Site 6 and may not apply more generically across the tested areas. However, the discussion above comparing the ground improvement results (shown in Figure 3) with the natural soil results relate to how the envelope of measured parameters for the ground improvements across all the sites have changed compared to the envelope of measured parameters for the natural soil sites. Therefore, these observations apply more generically across the tested areas in Christchurch and at some sites the site specific comparisons may indicate results that vary from the generic observations.

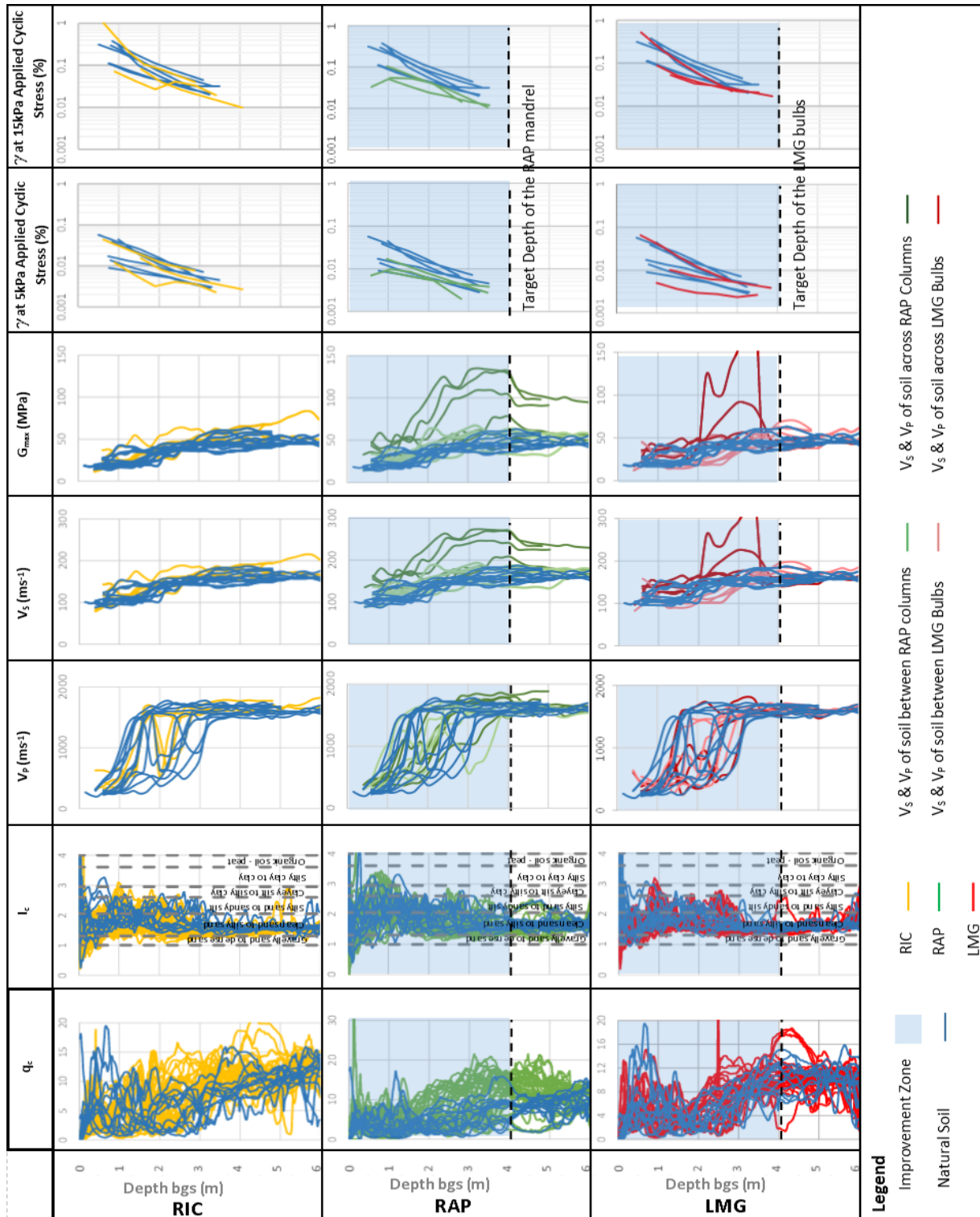


Figure 3. Natural soil and post-improvement  $q_c$  and  $I_c$  traces (first two columns) and crosshole  $V_p$  and  $V_s$  and corresponding  $G_{max}$  traces (middle three columns) for the natural soil and RIC, RAP and LMG ground improvements. Similarly, the last two columns show the vibroseis T-Rex  $\gamma$  traces at 5 and 15 kPa of applied cyclic horizontal stress at the ground surface.

The  $\gamma$  value at each PPT location for each load stage was converted into an equivalent Cyclic Stress Ratio (CSR) using the equation

$$CSR = \frac{\tau}{\sigma'_v} = \frac{G\gamma}{\sigma'_v} \quad (1)$$

where  $\tau$  is the cyclic shear stress (kPa),  $G$  is the shear modulus (kPa) of the soil which reduces with increasing  $\gamma$  and with decreasing  $\sigma'_v$  as the  $r_u$  increases during cyclic loading. The vertical effective stress (kPa) at each sensor location also includes the additional vertical stress from the applied vertical load imparted by the T-Rex truck during all dynamic testing.  $G$  is calculated from  $G_{\max} \times [G/G_{\max}] = \rho V_s^2 \times [G/G_{\max}]$ , where  $\rho$  is the soil density ( $\text{kg/m}^3$ ) and  $[G/G_{\max}]$  is a function of  $\gamma$  and  $\sigma'_v$  at each instant during loading using the measured pore pressures. The value of  $G$  is calculated using the procedures presented in Stokoe et al. (2016) using site-specific  $[G/G_{\max}]$ - $\log \gamma$  empirical relationships published in Menq (2003).

Figure 4 shows the calculated CSR values at each PPT location for all ground improvement panels for all sites at all loading stages are plotted against the representative composite  $V_s$  values that were inferred from the adjacent  $V_s$  tests (refer to Figure 2a). The  $V_s$  values were measured without the weight of the T-Rex truck in place so they were adjusted to account for the influence of the increased vertical load from the T-Rex truck.

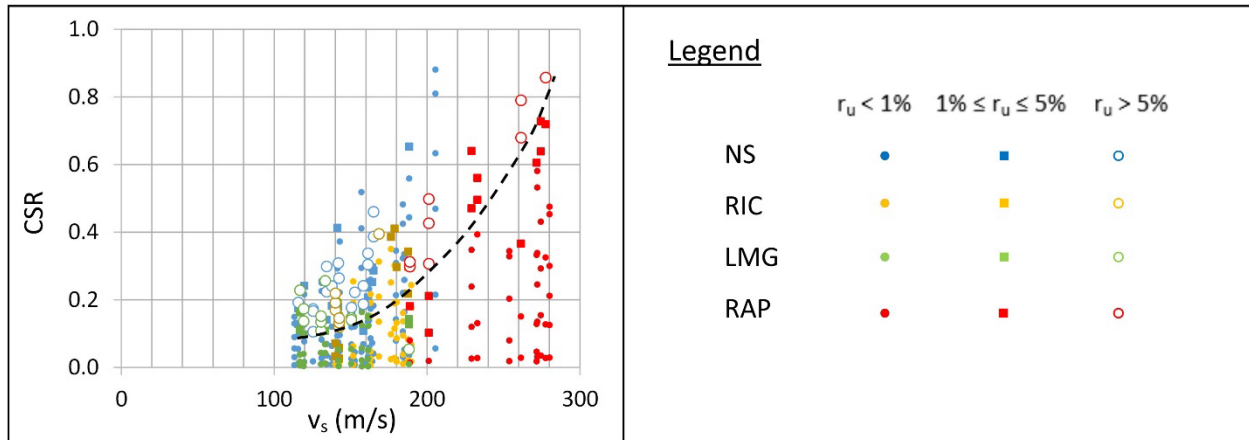


Figure 4. Calculated CSR values at each PPT location for all loading stages at all three trial sites for the Natural Soil (NS) and RIC, RAP and LMG ground improvements versus composite  $V_s$ .

The blue, yellow, green and red symbol colours identify the calculated natural soil CSR values for the Natural Soil (NS), RIC, RAP and LMG ground improvement panels, respectively. The solid dots represent calculated CSR values where the corresponding residual  $r_u$  at the end of the vibroseis T-Rex testing (indicated on Figure 2e) was  $< 1\%$ . Hollow circles represent calculated CSR values where the corresponding  $r_u$  was  $> 5\%$ . Solid squares represent CSR values where the  $r_u$  was between 1 and 5%. Only data points where the soil was close to complete saturation (assumed as  $V_p > 750$  m/s for the purposes of this study) are plotted on Figure 4 because, where the soils were not fully saturated, the development of  $r_u$  is likely to have been inhibited.

Figure 4 show that the onset of  $r_u$  development ( $r_u > 5\%$ ) for the nearly saturated soils ( $V_p > 750$

m/s) generally occurs at a CSR value of about 0.1 at low values of  $V_s$ . The CSR associated with a  $r_u > 5\%$  increases with increasing  $V_s$  (i.e. as the soil becomes stiffer the CSR required to generate  $r_u > 5\%$  increases). An illustration of this trend in terms of a potential boundary envelope is presented by the dashed line on Figure 4. This potential boundary does not represent a triggering boundary curve or a design curve as of now. It is simply presented to show the importance of raw  $V_s$  data in liquefaction triggering analyses.

Similar analyses were undertaken by normalizing the  $V_s$  data (i.e.  $V_{s1}$ ) using the Kayen et al. (2013) procedure. However, when the data were plotted, the  $V_{s1}$  did not separate the data as well as the raw  $V_s$ . Values of  $r_u > 5\%$  are important, because a slightly higher applied load, resulting in a slightly higher  $\gamma$ , causes  $r_u$  to rapidly increase resulting in liquefaction triggering as shown in Stokoe et al. (2014). Therefore, understanding the value of CSR at which  $r_u$  begins to rapidly develop is useful to determine whether liquefaction is likely or unlikely for a given CSR.

### **Discussion and Conclusions**

Ishihara (1985) recognised that a thick non-liquefying crust overlying liquefying soils would reduce the consequences of liquefaction (i.e., sand boils, loss of bearing capacity and differential settlement). This situation was confirmed by the observations following the CES, where less structural damage occurred in liquefaction-prone areas containing an intact, relatively stiff, non-liquefying crust with a minimum thickness of approximately 3 m. In-situ dynamic vibroseis T-Rex shake testing was undertaken on natural and RIC, RAP and LMG ground improvement panels to examine the liquefaction triggering to a depth of about 3 to 4 m below the ground surface, coinciding with the target depth of the ground improvement methods investigated as part of this study.

The vibroseis T-Rex testing of the ground improvement panels demonstrated that, in general, where the shallow ground improvements increased the CPT  $q_c$  (i.e. for the RAP ground improvement when  $I_c < 1.8$ ) or the composite crosshole  $V_s$  of the improved ground (i.e. for all  $I_c$  values for the RAP ground improvement) relative to the natural soil, there was a corresponding reduction in the  $\gamma$  in the improved soils and hence a potential improvement in the liquefaction resistance.

Conversion of the  $\gamma$  values into CSR values and plotting them against the corresponding raw  $V_s$  values, separated the cases of potential significant pore pressure generation ( $r_u > 5\%$ ) from cases of minimal pore pressure generation. Raw (i.e. un-normalised)  $V_s$  appears to separate clearly the CSR data points with  $r_u$  values of  $< 1\%$  and  $> 5\%$ . In particular, the RAP ground improvement panels exhibited this relationship, probably because  $V_s$  captures the stiffness of the composite soil-improvement element system. The CSR results demonstrate that, when the shallow ground improvements increase the composite crosshole  $V_s$  of the improved ground relative to the natural soil, the CRR of the soil increases, reducing the potential for liquefaction triggering.

### **Acknowledgments**

The experimental work described in this paper was funded by the New Zealand Earthquake Commission and was partially supported by U.S. National Science Foundation (NSF) grant

CMMI-1343524 and Graduate Research Fellowship Program (DGE-1110007). However, all findings and recommendations expressed in this paper are those of the authors and do not necessarily reflect the views of NSF. This support is gratefully acknowledged. The authors would also wish to acknowledge H Cowan and K Yamabe from the Earthquake Commission, Rick Fragaszy from the U.S. National Science Foundation and F. Menq, C. Hoffpauir, A. Valentine, R. Kent, Y. Wang, A. Stolte, and A. Keene, from the University of Texas at Austin.

## References

- Cox, B., Stokoe, K., & Rathje, E. (2009). An in-situ test method for evaluating the coupled pore pressure generation and nonlinear shear modulus behavior of liquefiable soils. *ASTM Geotechnical Testing Journal*, **32**(1), 11-21.
- Dobry, R., Ladd, R., Yokel, F., Chung, R., & Powell, D. (1982). *Prediction of Pore Water Pressure Buildup and Liquefaction of Sands During Earthquakes by the Cyclic Strain Method*. Washington, DC.: National Bureau of Standards.
- Ishihara, K. (1985). Stability of natural deposits during earthquakes. *Proceedings of the 11th International Conference on Soil Mechanics and Foundation Engineering. 1*, pp. 321-376. San Francisco: ISSMGE.
- Kayen, R., Moss, R., Thompson, E., Seed, R., Cetin, O., Kiureghian, A. D., . . . Tokimatsu, K. (2013). Shear wave velocity-based probabilistic and deterministic assessment of seismic soil liquefaction potential. *Journal of Geotechnical and Geoenvironmental Engineering, ASCE*, **139**, pp. 407-419.
- Menq, F.Y. (2003). *Dynamic properties of sandy and gravelly soils*. Ph.D. dissertation. The University of Texas at Austin.
- Rogers, N., van Ballegooy, S., Williams, K., & Johnson, L. (2015). Considering post-disaster damage to residential building construction - is our modern building construction resilient? *Proceedings of the 6th International Conference on Earthquake Geotechnical Engineering*. Christchurch, New Zealand: ISSMGE.
- Stokoe, K., Roberts, J., Cox, B., Hwang, S., Menq, F., & van Ballegooy, S. (2016). Effectiveness of shallow ground improvements to inhibit liquefaction triggering: methodology and analysis of field trials using controlled-source, dynamic loading with T-Rex. Submitted to *Soil Dynamics and Earthquake Engineering*.
- Stokoe, K., Roberts, J., Hwang, S., Cox, B., Menq, F., & van Ballegooy, S. (2014). Effectiveness of inhibiting liquefaction triggering by shallow ground improvement methods: Initial field shaking trials with T-Rex at one site in Christchurch, New Zealand. In Orense, Towhata, & Chouw (Eds.), *Soil Liquefaction During Recent Large-Scale Earthquakes* (pp. 193-202). London: Taylor & Francis Group.
- van Ballegooy, S., Wentz, F., Stokoe, K., Cox, B., Rollins, K., Ashford, S., & Olsen, M. (2015). *Christchurch Ground Improvement Trial Report*. Report for the New Zealand Earthquake Commission. (In press).
- Wentz, F., van Ballegooy, S., Rollins, K., Ashford, S., & Olsen, M. (2015). Large scale testing of shallow ground improvements using blast-induced liquefaction. *Proceedings of the 6th International Conference on Earthquake Geotechnical Engineering*. Christchurch, NZ: ISSMGE.
- Wansbone, M., & van Ballegooy, S., (2015). Horizontal Soil Mixed Beam Ground Improvement as a Liquefaction Mitigation Method Beneath Existing Houses. *Proceedings of the 6th International Conference in Earthquake Geotechnical Engineering*. Christchurch, New Zealand: ISSMGE.
- Wissmann, K., van Ballegooy, S., Metcalfe, B., Dismuke, J., & Anderson, C. (2015). Rammed aggregate pier ground improvement as a liquefaction mitigation method in sandy and silty soils. *Proceedings of the 6th International Conference on Earthquake Geotechnical Engineering*. Christchurch, New Zealand: ISSMGE.